Geotechnical and Geophysical Site Characterization – Huang & Mayne (eds)
© 2008 Taylor & Francis Group, London, ISBN 978-0-415-46936-4

SDMT-based deep excavation design

M. Arroyo & A. Di Mariano
Technical University of Catalunya, (UPC), Barcelona, Spain

P. Monaco
University of L'Aquila, Italy

M. Devincenzi & N. Pérez
Igeotest, Figueres, Spain

ABSTRACT: This communication presents some results from a case history in Barcelona involving a large cut-and-cover railway tunnel requiring a deep excavation (depth >20 m). Prediction of excavation-induced movements was necessary to assess third-party risk. A numerical model was set-up for the prediction and extrapolation of monitoring results obtained at a trial instrumented section. Monitoring results are here compared with model predictions relying mostly on results from seismic dilatometer tests (SDMT). Parameters deduced from dilatometric measures are employed to characterise the different soil layers using the Hardening soil model implemented in PLAXIS. Then, the extra information provided by the seismic data is fed into a nonlinear elastic-plastic model, using a well known stiffness-strain degradation curve. Results from both simulations are here compared with the monitoring data.

1 INTRODUCTION

Deep excavations in soils are inevitably associated with a certain amount of induced movement behind the excavation wall. While possibly inconsequential for the excavation itself, these movements might be damaging to any existing nearby structures. Therefore, assessment of the level of third-party risk associated with deep excavations in urban environments requires some knowledge of soil movements.

First estimates of movement can be made using empirical databases or simplified approaches that extrapolate predicted wall deflections. However, when the economical consequences of overestimating (or underestimating) induced damage are large, increased precision is welcome. It is then customary to resort to numerical methods that simulate the whole displacement field around the excavation, most commonly via a finite element discretization of the problem.

Numerical models "per se" do not guarantee any increase in predictive precision. There are many aspects in the numerical model of a deep excavation that require careful specification to achieve that objective. Correct initialization of the "in situ" stress state is one important example. There is little doubt that a good representation of the relevant mechanical soil behaviour is another.

One feature of soil behaviour that seems important when simulating excavation-induced movements is stiffness non-linearity at small strain levels. This has been consistently advocated by the Imperial College research group (e.g. Jardine et al., 1986; St John et al., 1993; Jardine et al. 2005) but also given support by many other researchers in the field (e.g. Brinkgreve et al. 2006).

To follow this approach, it is therefore necessary to obtain a stiffness degradation curve for the soils within the excavation profile. That has usually been obtained with laboratory tests incorporating small-strain measurement capabilities. However, these capabilities are still beyond the ability of many geotechnical laboratories. Moreover, for the small strain stiffness measurement to be meaningful high quality sampling is necessary. Unfortunately, high quality samples are simply not available in many circumstances, particularly when sandy or silty soils are involved.

In situ testing might be employed to skip the difficulties associated with the laboratory determination of the stiffness degradation curve. The self-boring pressuremeter (SBPM) has been successfully employed to establish the stiffness degradation curve of soils (Jardine, 1992; Fahey & Soliman, 1994). However, the SBPM is a highly specialised test, not as frequently available as it might be desired.

A possible alternative is offered by the combination of two stiffness measurements at very different stress levels. The dilatometer (DMT) offers one measure of stiffness at mid-strain levels. Seismic measurements would offer another stiffness measurement at small strain level. Seismic measurements might be independent (via cross-hole or SCPTu) or, more interestingly, simultaneous, thanks to the SDMT.

The approach outlined above has been already postulated to analyse foundation settlements in sand (Lehane and Fahey, 2004). Here will apply the same idea to a deep excavation on a mixed sand-clay profile. In the next section the basic geotechnical information of the case is given. Then the modelling approach employed is briefly described. Finally, monitoring results are compared with the model predictions and some conclusions are outlined.

2 CASE STUDY

2.1 *Project description*

The work here described refers to nearly 2.5 km of cut and cover tunnel corresponding to the high speed railway entry into Barcelona. The cut and cover works are located in plan between active railway lines and a densely populated residential area. Amongst other buildings, a number of 14-storey residential towers are aligned at distances varying between 2 and 15 m from the retaining wall. The excavation depth near the built area varies between 15 and 25 m

The general construction method involves a top-down construction. Movement at the top of the wall is restrained using concrete beams, below it several provisional steel bracings are employed while the tunnel vault is constructed. Afterwards the bracing is retired while earth filling above the vault, and the tunnel is excavated to counter-vault level, again with help of some provisory steel bracing. Additional measures in difficult areas might include buried jet-grouted slabs, additional steel bracing and the substitution of concrete beams by continuous slabs and/or retaining walls by piles (in this later case to minimize installation associated movements).

To minimize the cost of the additional measures a staged risk-assesment procedure was established (Arroyo et al. 2007). The advanced analysis stage was based on detailed numerical modelling of the excavation, supported and contrasted by the monitoring results obtained at trial excavation sections located in no-built areas.

Results from one of these trial sections, already excavated to maximum depth are here employed to check the ability of DMT/SDMT data to obtain displacement predictions. Conditions at this trial excavation section are next described.

Table 1. Stratigraphic model at the trial excavation section.

Level ID	Description	Thickness (m)	Bottom depth (m)
N0	Made ground	3.5	3.5
N1	Silty clay	3	6.5
N2A	Coarse sand	5	11.5
N2B	Fine sand	10.5	22
N3	Silt	11.5	33.5
N4	Gravel	5	38.5

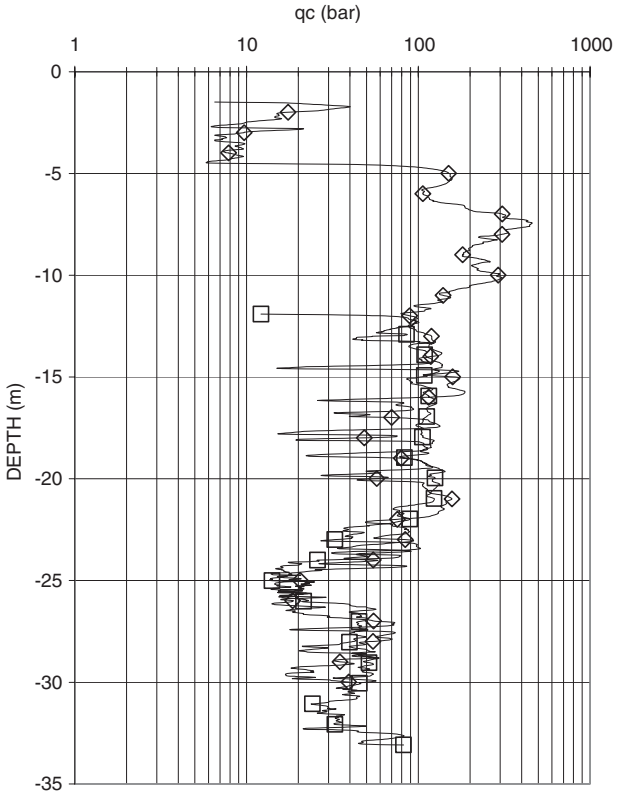

Figure 1. Cone point resistance profiles near the trial excavation section at Rampa 1.

2.2 *Trial excavation section*

The trial excavation section (Rampa1) takes place in deltaic deposits. Deltaic deposits are layered sub-horizontally and include, from top to bottom, clay, sand, silt and gravelly sand. Silts and clay are soft, whereas the granular layers are rigid and somewhat cemented by carbonates, occasionally resulting on thin hardpans. The deltaic deposits are overlaid by several meters of made ground and overlie a stiff marly clay deposit of Pliocene age. Table 1 gives the details of the soil profile at the trial section. Figure 1 reproduces cone resistance profiles from nearby probes. The profiles reveal clearly the contrast between the strong sands above and the soft silts below.

At the trial section the maximum excavation depth is 16 m. The concrete retaining wall has a thickness of 0.8 m and depth of 27 m. The water table is located at 9 m depth. The original ground level is at about 7 m above the reference sea level.

Monitoring at the trial section included extensometers and pressure cells on the tunnel structural elements and the wall, inclinometers at the retaining wall, surface topography and three multiaxial extensometers behind the wall.

2.3 *DMT and SDMT testing*

Geotechnical exploration at the site included a large number of boreholes, laboratory testing, cross-hole, CPTu and DMT sounding and a number of self-boring pressuremeter tests. Soil characterization for design was based on all the information available.

However, for the purposes of the simulation exercise here described, all the information available from sources other than the DMT and SDMT soundings, was deliberately ignored. The only exceptions were made with the water table location, soil density and permeability. Also, at depths where these tests results were unavailable the DMT/SDMT information was complemented with other tests, as explained below.

It was initially planned to obtain a continuous SDMT measurement up to the top of the gravel layer or 35 m depth. However, the presence of cemented pans on the coarse sand layer (see Figure 1 at 6 m depth) made it impossible, because the DMT pushing rods were unable to withstand the force necessary to penetrate these layers. The first test (SDMT A R1) was therefore stopped at 6 m depth. A second probe (SDMT B R1) was then made, using a 6 m pre-bored 400 mm borehole, filled with sand. This probe advanced 12 m, up to before an alignment problem with the impact equipment for the seismic signal meant the end of the test. Finally, a third probe (DMT C R1) was performed up to 35 mm depth, this time starting at a depth of 11 m from within the excavation. This last probe had no seismic capability.

The DMT readings are shown in Figure 2. It is interesting to look in detail at the readings in the area where SDMT B R1 (made from the surface) and DMT C R1 (made from the excavation bottom) overlap, Figure 3. The p_0 and p_1 lectures of the probe made from the excavation bottom are systematically below those made from the surface; however, their difference, $p_0 - p_1$, is very similar for both probes. This means that the E_D and I_D values are almost unaffected, whereas the K_D value, directly related to OCR and K0, changes to reflect the excavation unloading.

Shear velocity measurements are shown in Figure 4, alongside results from a nearby cross-hole test. At the depths where both tests overlap there are large discrepancies. SDMT measures seem more reliable, because

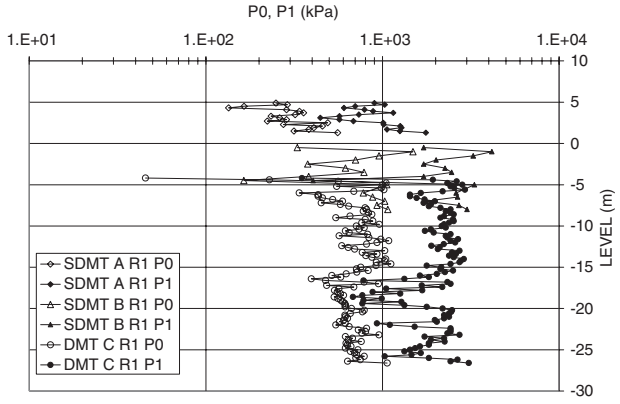

Figure 2. P0 and P1 readings from DMT's at Rampa 1.

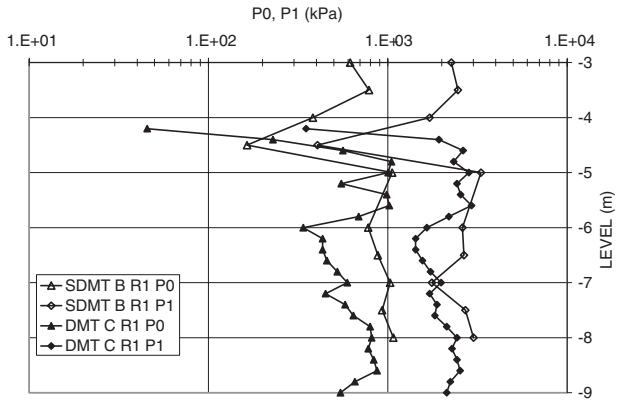

Figure 3. Detail of the dilatometer readings.

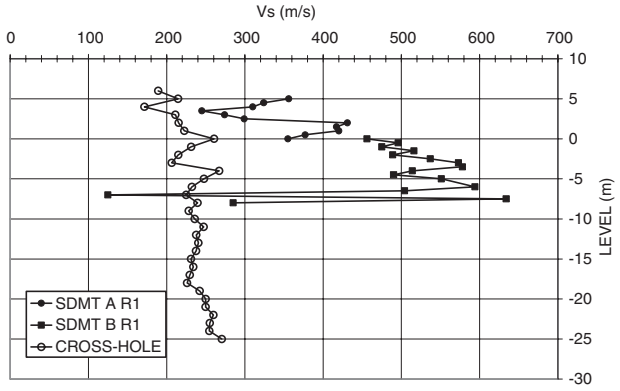

Figure 4. Shear velocity measurements from SDMT and cross-hole results.

it reveals multiple layers of contrasted stiffness, which seems more likely considering other measures, like cone resitance (Figure 1). Also, the cross-hole was performed with a single-receiver configuration, which makes the test more error-prone. For these reasons, the cross-hole measurements are here employed only where there is lack of SDMT measures.

Table 2. Common parameters for all models. DMT-based values for simulation.

Level	K0	s_u (kPa)	ϕ	Ψ
N0	0.5	–	36	6
N1	0.8	38	–	–
N2A	0.5	–	38	8
N2B	0.5	–	35	5
N3	0.5	68 (120)	–	–

Table 3. HSM model. DMT based parameters for simulation.

Level	E_{oed}^{ref} (MPa)	E_{oed}^{ref} (MPa)	E_{oed}^{ref} (MPa)	m	υ_{ur}
N0	44.7	44.7	178.9	0.5	0.2
N1	13.9	13.9	55.6	0.5	0.2
N2A	85.3	85.3	341.2	0.5	0.2
N2B	54.7	54.7	218.6	0.5	0.2
N3	8.4	8.4	33.7	0.5	0.2

3 EXCAVATION MODELLING

3.1 *General features*

A finite element model of the excavation works was set up using the commercial code PLAXIS. The model included both excavation sides, as the surface loads and final ground levels were asymmetric. A ten-step constructive sequence was modelled, including the application of surface loads, four intermediate excavation steps, two provisional support levels, the execution of the tunnel vault and countervault and progressive water table lowering inside the excavation. The model included about 2500 fifteen-noded elements and typically resulted in somewhat cumbersome runs (from several hours up to several days for the small strain model described below) in a 1.2 GHz Centrino Duo computer.

Levels N1 and N3 were set up as undrained, although the excavation sequence allowed for consolidation periods of between 10 and 15 days at each major stage. Stress initialization was done using the DMT deduced K0 values featured in Table 2.

Two different constitutive models, explained below, were employed to characterize the soil layers. Though different, both models are elasto-plastic and share the description of plastic failure. The relevant parameters for granular (friction angle, ϕ) and cohesive layers (undrained shear strength, s_u) were estimated using the usual dilatometric correlations and are detailed in Table 2. The dilatancy angle, Ψ, was estimated from the friction angle. Level N4 was not recognized by DMT and has anyway very little presence in the numerical models later described.

In the table above two different values are assigned to the undrained shear strength of the silts at N3. The lower value is the one deduced from the DMT readings, based on previous SBPM information, was that finally adopted. This was done because there were doubts about how representative was the DMT measure, obtained from within the excavations, of conditions prior to it or outside the walls.

3.2 *Hardening soil model*

The hardening soil model (Schanz et al., 1999) is an elasto-plastic model, featuring non-linear elasticity and two plastic mechanisms. The model has three stiffness controlling parameters. Two of them relate to plastic deformation: a tangent oedometer modulus E_{oed}^{ref} and a secant triaxial modulus E_{50}^{ref}. Elastic deformation requires the specification of an unloading-reloading modulus E_{ur}^{ref}, plus a Poisson ratio. These parameters are employed to specify stress-level dependent moduli, according to:

$$E_{oed} = E_{oed}^{ref}\left(\sigma_1'/p^{ref}\right)^m$$
$$E_{50} = E_{50}^{ref}\left(\sigma_3'/p^{ref}\right)^m \quad (1)$$
$$E_{ur} = E_{ur}^{ref}\left(\sigma_3'/p^{ref}\right)^m$$

σ_1' and σ_3' stand for major and minor principal effective stresses, and p^{ref} is a reference pressure, usually taken as 100 kPa.

Monaco & Marchetti (2004) explain how the dilatometer modulus, M_{DMT}, might be employed as the basic reference stiffness parameter. A first assumption, quite reasonable if previous results of surface settlement evaluation are taken into account, is $E_{oed} = M_{DMT}$. A second, more stringent assumption, is that $E_{50}/E_{oed}/E_{ur}$ maintain approximately the proportion 1/1/4 for all soil layers.

For homogeneous soil layers the profile of M_{DMT} might be employed to establish both m and E_{oed}^{ref}. In this case the marked heterogeneity of the soil profile required another approach. A value of $m = 0.5$ was assumed for all layers and a profile of E_{oed}^{ref} was obtained. This profile was then simplified, assigning a single E_{oed}^{ref} value to each layer. Care was taken to ensure that the simplification thus introduced did not change the equivalent vertical compressibility of each layer. The resultant model parameters are collected in Table 3.

3.3 *Small strain model*

Jardine et al. (1986) proposed a non-linear elastic model for soil behaviour. Here, the effective stress version of this model (e.g. Jardine et al., 2005) is

Table 4. Small strain model. DMT based parameters for simulation.

Level	A	B	C (%)	α	γ	ε_{Dmin} (%)	ε_{Dmax} (%)
N1	562	540	1e-4	1.45	0.62	1.7e-3	0.34
N2A	646	604	1e-4	1.33	0.62	1.7e-3	0.34
N2B	503	473	1e-4	1.4	0.62	1.7e-3	0.34
N3	194	186	1e-4	1.45	0.62	1.7e-3	0.34

employed. The secant shear and bulk modulus are formulated as

$$\frac{G_{sec}}{p'} = A + B\cos\left[\alpha\left(\log_{10}\left(\frac{E_d}{\sqrt{3C}}\right)\right)^{\gamma}\right]$$
$$\frac{K_{sec}}{p'} = R + S\cos\left[\delta\left(\log_{10}\left(\frac{|\varepsilon_v|}{T}\right)\right)^{\eta}\right] \quad (2)$$

where A, B, C, α, γ, R, S, T, δ, η are model adjustment parameters. The secant modulus are made explicitly dependent on the following invariant measures of strain

$$E_d = \frac{2}{\sqrt{6}}\sqrt{(\varepsilon_1-\varepsilon_2)^2+(\varepsilon_2-\varepsilon_3)^2+(\varepsilon_1-\varepsilon_3)^2} \quad (3)$$
$$\varepsilon_v = \varepsilon_1+\varepsilon_2+\varepsilon_3$$

The expressions in (2) are only valid for restricted ranges of the strain variables (3) also to be specified.

To calibrate this model on SDMT data a number of simplifications and assumptions were made. First, it was assumed that the secant bulk modulus and secant shear modulus degradation curves were identical – equivalent to a strain-independent Poisson ratio of 0.12. Then, the secant shear modulus vs shear strain curve was fitted at two points, one given by the dilatometric modulus M_{DMT} and the other by the shear velocity of each layer.

The dynamic modulus was assigned a shear strain level of around 1E-3%. The dilatometric modulus is assigned to a strain range between 5 and 10E-2%, following suggestions of Mayne (2001) and Ishihara (2001), but well below the range suggested by Lehane & Fahey (2004). Curve adjustment was made using only three parameters (A, B, α) at each level; the others were assigned constant values for all the profile (Table 4).

4 SIMULATION RESULTS

At the time of writing the excavation works were not complete; however there were enough results already available from the monitoring to make a comparison

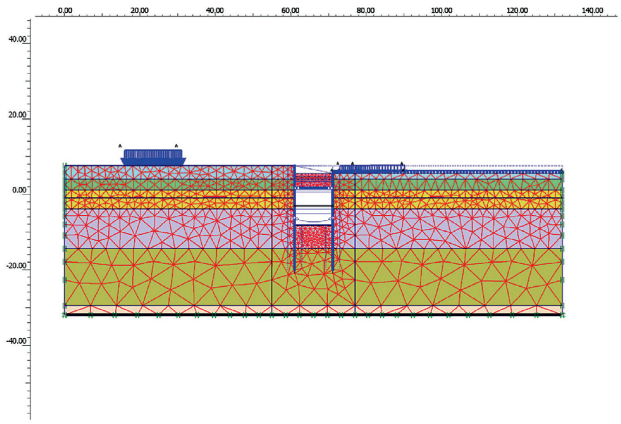

Figure 5. General view of the numerical model of the trial excavation at the maximum excavation depth stage.

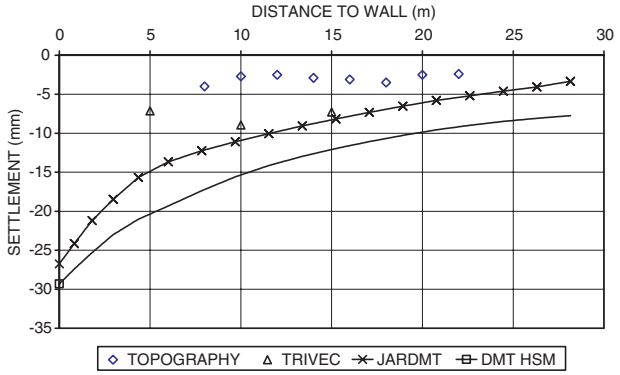

Figure 6. Surface settlements behind the wall. Monitoring results and model predictions.

with model predictions worthwhile. The measurements now presented will all correspond to a phase in which the tunnel excavation has reached maximum depth, but where the countervault has not yet being laid (Figure 5).

Since the concern here is with the ability to forecast excavation-induced third-party risk, we will deal only with the directly relevant results, i.e. movements of the ground behind the wall. These were observed on the surface using topography and, through multiaxial extensometers or Trivec, at three vertical lines, located at 5, 10 and 15 m behind the wall.

4.1 *Settlement*

Figure 6 represents the settlements at the surface. The predictions from the small strain model lie very close to the Trivec measurements at distances of 10 and 15 m behind the wall and below the surface monitoring results. The hardening soil model predicts larger settlements, and it is therefore farther from the measures.

Figure 7 reveals a more detailed picture of the settlement prediction. The results of the small strain model

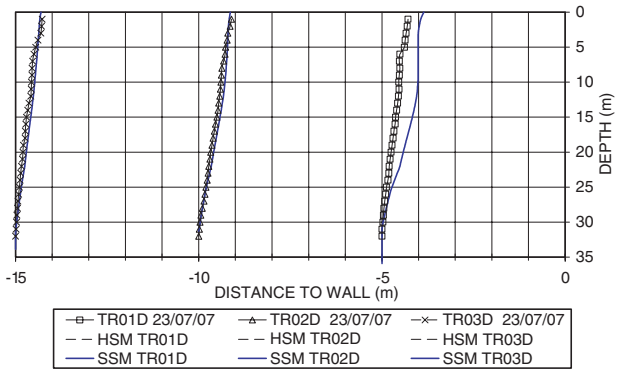

Figure 7. Displacements towards the wall at various vertical alignments. Displacements scaled by a 100 factor. Monitoring results (symbols). HSM predictions (thin lines). SSM predictions (thick lines).

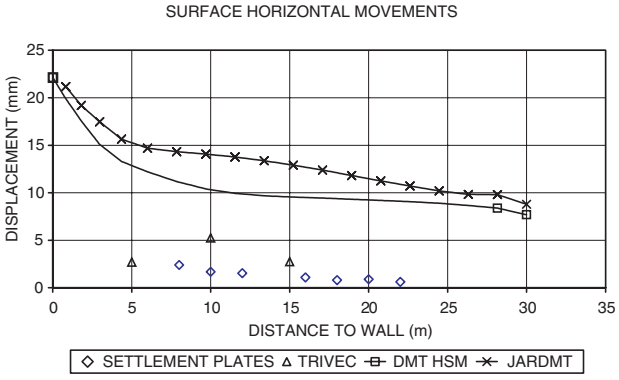

Figure 8. Surface displacements towards the wall. Monitoring results and model predictions (HSM squares; SSM crosses).

are remarkably close to the measurements at the two instruments farther away from the wall. Discrepancies in the hardening soil model predictions seem to be more pronounced in the deeper layers. This might be due to a somewhat conservative idealization of the geotechnical profile (compare Figure 1 and Table 1).

The best performance of the model incorporating small strain stiffness information for settlement was expected (Jardine et al. 2005, Brinkgreve et al. 2006).

4.2 *Horizontal displacements*

The comparison of predicted and measured horizontal displacements is less favourable. Both models overpredict, by a factor of 2 or more, the movements on the surface (Figure 8). The small strain model has a larger error than the hardening soil model, something that was unexpected.

When the distribution of horizontal movements with depth is considered (Figure 9) it is apparent that the larger errors in the small strain model appear on the deeper layers, whereas the error in the hardening soil model prediction is more uniformly distributed.

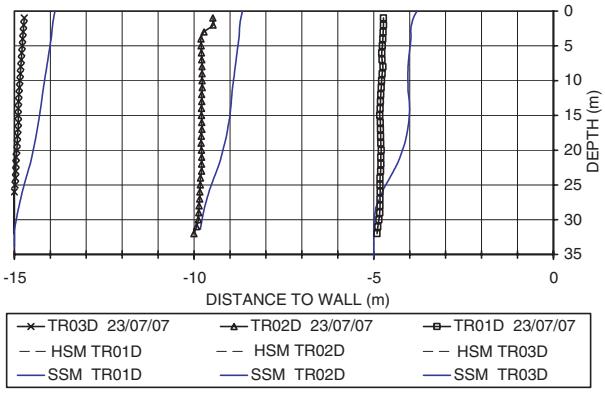

Figure 9. Displacements towards the wall at various vertical alignments. Displacements scaled by a 100 factor. Monitoring results (symbols). HSM predictions (thin lines). SSM predictions (thick lines).

5 CONCLUSIONS

It is worth mentioning, that, despite erring on the safe side, the numerical model predictions resulted in far lower risk estimates for neighbouring structures than those made initially using simplified methods (see Arroyo et al. 2007).

However, the main lesson that might be drawn from the case here presented is that it is possible to rely on DMT/SDMT obtained information to model excavation induced movements with a fair degree of accuracy. A secondary lesson is that (S)DMT measures below indurated layers are possible, but require good planning of the associated fieldwork.

ACKNOWLEDGMENTS

The support of ADIF and UTE Hospitalet (OHL-Guinovart) for the performance of the work reported in this paper is gratefully acknowledged. Dr. M. Rouainia, from the University of Newcastle upon Tyne, coded the small-strain model into Plaxis.

REFERENCES

Arroyo, M., DiMariano, A., Gens. A, Alonso, E., García Fontanet, A. & García Germán, J. (2007) Management of third-party risk in an urban deep excavation project, *XIV European Conf. of Soil Mech, Geotech. Eng.*, Madrid (to appear)

Brinkgreve, R.B.J., Bakker, K.J. & Bonnier, P.G. (2006) The relevance of small-strain soil stiffness in numerical simulation of excavation and tunneling projects, in *Numerical methods in Geotechnical Engineering – Schweiger (ed.)* 133–139.

Fahey, M. & Soliman, A.A. (1994) Measuring the small-strain behaviour of sand in situ. *Pre-Failure Deformation*

Characteristics of Geomaterials (IS–Hokkaido), Sapporo, Japan, Balkema, Rotterdam, Vol. 1, 217–222.

Ishihara, K. (2001) Estimate of relative density from in-situ penetration tests. *Proc. Int. Conf. on In Situ Measurement of Soil Properties and Case Histories, Bali*, 17–26.

Lehane, B. & Fahey, M. (2004) Using SCPT and DMT data for settlement prediction in sand, *Proc. ISC-2 Geotechnical and Geophysical Site Characterization, Viana da Fonseca & Mayne (eds.)*, Vol. 2, 1673–1679.

Jardine, R.J., Potts, D.M., Fourie, A.B. & Burland, J.B. (1986) Studies of the influence of non-linear stress-strain characteristics in soil-structure interaction, *Geotechnique*, 36, 3, 377–396.

Jardine, R.J. (1992) Nonlinear undrained parameters from undrained pressuremeter tests, *Can. Geotech. J.*, 29, 436–447.

Jardine, R.J., Standing, J.R. & Kovacecic, N. (2005) Lessons learned from full scale observations and the practical application of advanced testing and modeling, in *Deformation Characteristics of Geomaterials – Di Benedetto et al (eds.)* Taylor & Francis, London, Vol. 2 201–245.

Mayne, P.W. (2001) Stress-strain-strength-flow parameters from enhanced in-situ tests. *Proc. Int. Conf. on* In Situ *Meas-urement of Soil Properties and Case Histories, Bali*, 27–47.

Monaco, P., Totani, G. & Calabrese, M. (2006) DMT-predicted vs observed settlements: a review of the available ex-perience. *Proc. 2nd Int. Conf. on the Flat Dilatometer, Washington D.C.*, 244–252.

Monaco, P. & Marchetti, S. (2004) Evaluation of the coefficient of subgrade reaction for design of multipropped diaphragm walls from DMT moduli, *Proc. ISC-2 Geotechnical and Geophysical Site Characterization, Viana da Fonseca & Mayne (eds.)*, Vol. 1, 993–1002.

Schanz, T., Vermeer, P.A. & Bonnier, P.G. (1999) The hardening soil model: formulation and verification, Beyond 200 in Computational geotechnics – 10 Years of PLAXIS, Balkema, Rotterdam. 1–16.

St John, H.D., Potts, D.M., Jardine, R.J. & Higgins, K.G. (1993) Prediction and performance of ground response due to construction of a deep basement at 60 Victoria Embankment, *In Predictive Soil Mechanics*, Thomas Telford, London, 581–608.